JACS
JOURNAL OF THE AMERICAN CHEMICAL SOCIETY
Article
pubs.acs.org/JACS

Electron Transfer Kinetics in CdS Nanorod–[FeFe]-Hydrogenase Complexes and Implications for Photochemical H_2 Generation

Molly B. Wilker,[†] Katherine E. Shinopoulos,[†] Katherine A. Brown,[‡] David W. Mulder,[‡] Paul W. King,[‡] and Gordana Dukovic*[,†]

[†]Department of Chemistry and Biochemistry, University of Colorado Boulder, Boulder, Colorado 80309, United States
[‡]Biosciences Center, National Renewable Energy Laboratory, Golden, Colorado 80401, United States

Supporting Information

ABSTRACT: This Article describes the electron transfer (ET) kinetics in complexes of CdS nanorods (CdS NRs) and [FeFe]-hydrogenase I from *Clostridium acetobutylicum* (CaI). In the presence of an electron donor, these complexes produce H_2 photochemically with quantum yields of up to 20%. Kinetics of ET from CdS NRs to CaI play a critical role in the overall photochemical reactivity, as the quantum efficiency of ET defines the upper limit on the quantum yield of H_2 generation. We investigated the competitiveness of ET with the electron relaxation pathways in CdS NRs by directly measuring the rate and quantum efficiency of ET from photoexcited CdS NRs to CaI using transient absorption spectroscopy. This technique is uniquely suited to decouple CdS→CaI ET from the processes occurring in the enzyme during H_2 production. We found that the ET rate constant (k_{ET}) and the electron relaxation rate constant in CdS NRs (k_{CdS}) were comparable, with values of 10^7 s^{-1}, resulting in a quantum efficiency of ET of 42% for complexes with the average CaI:CdS NR molar ratio of 1:1. Given the direct competition between the two processes that occur with similar rates, we propose that gains in efficiencies of H_2 production could be achieved by increasing k_{ET} and/or decreasing k_{CdS} through structural modifications of the nanocrystals. When catalytically inactive forms of CaI were used in CdS–CaI complexes, ET behavior was akin to that observed with active CaI, demonstrating that electron injection occurs at a distal iron–sulfur cluster and is followed by transport through a series of accessory iron–sulfur clusters to the active site of CaI. Using insights from this time-resolved spectroscopic study, we discuss the intricate kinetic pathways involved in photochemical H_2 generation in CdS–CaI complexes, and we examine how the relationship between the electron injection rate and the other kinetic processes relates to the overall H_2 production efficiency.

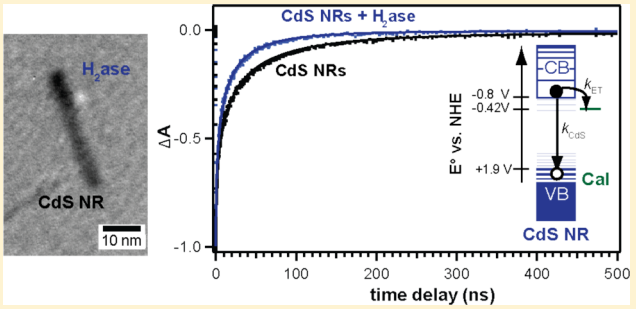

INTRODUCTION

Colloidal semiconductor nanocrystals are excellent model light harvesting elements for artificial photosynthesis because they are strong light absorbers with tunable particle size, shape, electronic structure, absorption spectra, and surface chemistry.[1−7] In recent years, semiconductor nanocrystals have been coupled with a variety of redox catalysts in solution-phase nanoarchitectures that use visible light to drive reduction of two protons to produce H_2.[7,8] The catalysts include noble metal nanoparticles,[9−15] transition metal complexes,[16,17] enzymes,[18−22] and molecular mimics of enzyme active sites.[23−26] In this Article, we focus on the coupling of nanocrystals with hydrogenase, a remarkable biological catalyst that can reversibly generate H_2 very close to the thermodynamic potential.[27−31] Hydrogenases utilize redox cofactors composed of earth-abundant elements (Fe, Ni, S) for electron transport and catalysis. [FeFe]-hydrogenases, in particular, exhibit high catalytic activities for H^+ reduction to H_2.[32,33] In nature, H_2 generation catalyzed by [FeFe]-hydrogenases requires injection of low-potential electrons from ferredoxin (Fd) to a distal accessory [4Fe–4s] cluster (F-cluster) near a positively charged surface patch of the enzyme.[34−37] Electron injection is followed by electron transport through F-clusters to the active site (H-cluster), where two protons are reversibly reduced to H_2.[38−40] It is thought that the active sites of [FeFe]-hydrogenases have metastable 1-electron reduced states that can persist until a second electron arrives and H_2 is generated.[41−43]

We recently demonstrated that complexes of CdS nanorods (NRs) and [FeFe]-hydrogenase from *Clostridium acetobutylicum* (CaI) generate H_2 under illumination, with quantum yields ($QY(H_2)$) of up to 20% at a CaI:CdS NR molar ratio of ~1:1.[19] $QY(H_2)$ is defined as (H_2 molecules produced/photons absorbed) × (2 electrons/H_2 molecule).[19] CaI exhibits high catalytic activity with turnover frequencies (TOFs) up to ~10^4 (H_2 molecules)/(enzyme × s).[44] The CdS–CaI complexes form via a biomimetic interaction in which CdS NRs, capped with negatively charged surface ligands, bind to CaI as analogues of the electron-donating protein Fd.[18,19] We

Received: December 26, 2013
Published: February 24, 2014

   dx.doi.org/10.1021/ja413001p | J. Am. Chem. Soc. 2014, 136, 4316–4324

proposed a model for photochemical H_2 generation that involves light absorption by CdS NRs and injection of photoexcited electrons (i.e., electron transfer (ET)) into CaI, which can then utilize two electrons to reduce two protons and generate one H_2 molecule (Figure 1).[19] Holes are removed by the electron donor ascorbate ($AscH^-$).[45] The biomimetic binding interaction suggests that the electrons injected from CdS should follow the biological pathway, with electron injection at a distal F-cluster followed by electron transport to the H-cluster.[18,19,21,44,46]

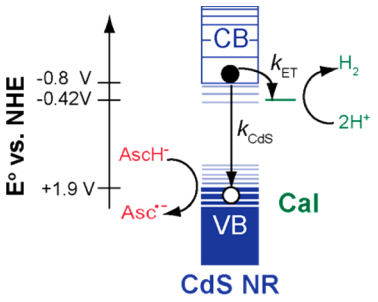

Figure 1. Energy level diagram depicting the processes required for photochemical H_2 generation by CdS−CaI complexes. Photoexcitation of CdS is followed by electron transfer from CdS to CaI, denoted with the rate constant k_{ET}. Two electrons are utilized for the reduction of $2H^+$ to H_2. Holes are scavenged by the electron donor ascorbate ($AscH^-$). k_{CdS} represents the rate constant for electron decay pathways in the CdS NRs, including radiative and nonradiative recombination and carrier trapping. These processes compete with ET. Energy levels shown in light blue symbolize the electron and hole trap states.

Critical to our understanding of photochemical H_2 generation in CdS−CaI complexes is the fact that electron relaxation pathways in CdS NRs, such as trapping and recombination, are in kinetic competition with ET to CaI (Figure 1). The quantum efficiency of ET to CaI (QE_{ET}), defined as (electrons transferred)/(photons absorbed), depends on the ratio of the ET rate constant (k_{ET}) and the rate constant of the internal electron decay processes (k_{CdS}). The value of QE_{ET} defines the upper limit on the value of $QY(H_2)$ because only electrons delivered to CaI can be incorporated into H_2 molecules. The measured value of $QY(H_2)$ will be lower than that of QE_{ET} if there are subsequent rate-limiting processes in H_2 generation. To understand the factors that determine QE_{ET}, its relationship to $QY(H_2)$, and to propose strategies for the improvement of H_2 production efficiency, it is necessary to directly measure the values of k_{ET} and k_{CdS}.

In this Article, we describe the first measurements of rates and efficiencies of ET between photoexcited CdS and CaI in CdS−CaI complexes using transient absorption (TA) spectroscopy. We found that both electron relaxation in CdS NRs and CdS→CaI ET proceed relatively slowly, with rate constants k_{CdS} and $k_{ET} \approx 10^7\ s^{-1}$, resulting in a QE_{ET} of 42% when the molar ratio of CaI to CdS NRs is 1:1. We attribute the relatively low value of k_{ET} to the nature of the CdS−CaI interface, which requires electron tunneling over a considerable distance. We found that the rate of electron removal from CdS NRs increases linearly with increasing numbers of enzyme moieties per NR; however, the $QY(H_2)$ decreases as multiple CaI compete for electrons. To probe the pathway of an electron injected into CaI, we performed TA measurements on CdS−CaI complexes with catalytically inactive CaI, which were not capable of generating H_2. Such complexes exhibited ET behavior similar to that of complexes of CdS NRs with catalytically active CaI, confirming that the electron trajectory in CdS−CaI complexes is analogous to the natural pathway that electrons follow in [FeFe]-hydrogenases after injection from Fd. To increase the fraction of photoexcited electrons delivered to CaI, we propose that both decreasing k_{CdS} and increasing k_{ET} would be beneficial due to their almost equivalent values. Both goals may be achievable via tuning of the nanocrystal structure. The rate of electron transport through CaI, which occurs after electron injection, defines the upper limit on the value of k_{ET} that would be beneficial to H_2 generation efficiency. We conclude our discussion by contrasting the ET kinetics and H_2 production in CdS−CaI complexes with the behavior of CdS−Pt nanoheterostructures that also photochemically produce H_2. Our study of ET kinetics in CdS−CaI complexes allows us to elucidate how the electron injection step from the nanocrystal to the enzyme governs the overall H_2 production efficiency, and provides a first glimpse into the intricate kinetics of photochemical H_2 generation in nanocrystal−enzyme biohybrids.

EXPERIMENTAL SECTION

Sample Preparation. *CdS Nanorods.* CdS NRs were synthesized according to previously reported methods.[19,47−49] The resulting NRs had an average diameter of 4.3 ± 0.4 nm and an average length of 21.5 ± 5.2 nm for sample CdS α or an average diameter of 4.4 ± 0.6 nm and an average length of 32.0 ± 5.8 nm for sample CdS β, as determined by measurements of over 200 particles in TEM images (Supporting Information Figure S1). The molar absorptivity (ε) of the CdS NRs was determined by correlating absorption spectra with Cd^{2+} concentrations determined by elemental analysis (ICP-OES) of acid-digested samples. The estimated value of ε_{350} was 1710 $M^{-1}\ cm^{-1}$ per Cd^{2+}. The number of Cd^{2+} per NR was estimated from the average NR dimensions. ε_{350} was $1.1 \times 10^7\ M^{-1}\ cm^{-1}$ for CdS α and $1.7 \times 10^7\ M^{-1}\ cm^{-1}$ for CdS β. The hydrophobic surface-capping ligands on the as-synthesized CdS nanorods were replaced with 3-mercaptopropionic acid (3-MPA) following a previously reported procedure.[10,19,47] 3-MPA binds to the NR surface through the deprotonated thiol group, leaving the carboxylate group in solution to enable solubility in water.[50] All of the procedures described above were carried out under an Ar atmosphere.

CaI and CaI^{Im} Purification, Characterization, and Coupling to CdS NRs. The StrepII-tagged [FeFe]-hydrogenase from *Clostridium acetobutylicum* (CaI) was expressed and purified from *Escherichia coli* as previously described.[51] Catalytically inactive CaI lacking the diiron subsite ($2Fe_H$) of the H-cluster (CaI^{Im}) was prepared by expression in a genetic background lacking the maturation proteins HydE, HydF, and HydG.[52,53] Cells were harvested in an anaerobic chamber (Coy Laboratories) under 3% H_2 atmosphere. CaI purification was carried out under strict anaerobic conditions in a glovebox (MBRAUN Laboratory Products) under a N_2 atmosphere. In the final Strep-Tactin purification step, CaI was eluted in 50 mM Tris-HCl pH 8.0, 200 mM NaCl, 5% glycerol, and 5 mM sodium dithionite (NaDT). The CaI concentration was determined by Bradford assay (±10%). Typical yields were 1−2 mg/L of culture with specific activities between 800 and 1300 μmol H_2/mg/min. CaI activities were determined by measuring H_2 evolution on a gas chromatograph (Agilent Technologies) after addition of 5 mM methyl viologen and 10 mM NaDT. For CaI^{Im}, the Fe content was confirmed on a separate preparation using a colorimetric assay described by Fish.[54]

Mixtures of CdS NRs and CaI were prepared in buffer (50 mM Tris-HCl, 5 mM NaCl, 5% glycerol, pH 7) under an anaerobic Ar environment. To prepare CdS−CaI^{CO}, the CdS NRs and CaI were first mixed under Ar in a 2 mm cuvette modified with an airtight Kontes valve and a glass side arm. The headspace was exchanged for CO by flowing CO (99.99%, Airgas) into the cuvette for 30 min while stirring the sample solution. The sample was then sealed with 0.8 atm

dx.doi.org/10.1021/ja413001p | J. Am. Chem. Soc. 2014, 136, 4316−4324

CO (atmospheric pressure in Boulder, Colorado) in the cuvette headspace. When the CaI:CdS NR ratio was varied, the concentration and absorbance of the NRs were held constant while the concentration of CaI was varied.

Sample Characterization. *Steady-State Absorption Spectroscopy.* UV−visible absorption spectra were recorded in 2 mm path length quartz cuvettes at room temperature with an Agilent 8453 spectrophotometer equipped with tungsten and deuterium lamps.

Transmission Electron Microscopy (TEM). TEM samples of CdS NRs were prepared by drop casting from solution onto carbon film, 300 mesh, copper grids from Electron Microscopy Sciences. Images were obtained at room temperature using a Phillips CM100 TEM operating at 80 kV equipped with a bottom-mounted 4 megapixel AMT v600 digital camera. NR dimensions were measured using ImageJ software.[55] To prepare CdS−CaI samples for TEM imaging, the grids were first plasma-treated by glow discharge. A drop of a dilute (nM) solution of CdS β NRs and CaI was then placed onto the grids for 2 min, after which the solvent was wicked away using filter paper. The grids were rinsed with deionized water in the same manner before being stained in H_2O with 2% methylamine vanadate negative stain (NanoVan, Nanoprobes Inc.), which was wicked away in <10 s. In a negatively stained image, the electron-dense material (CdS) appears dark in contrast to the stained background, while CaI appears light in contrast to the background.

Transient Absorption Spectroscopy. The TA experimental setup was previously described in detail.[47] The samples were prepared and sealed under Ar in 2 mm quartz cuvettes modified with airtight Kontes valves. CdS NR concentration was 600−800 nM. The samples containing both NRs and CaI were mixed in specific molar ratios in 50 mM Tris-HCl buffer without a hole scavenger. The samples were pumped at 400 nm. The pump beam diameter was ∼240 μm, and the pulse energy was ∼10 nJ/pulse. Pump power was chosen by identifying a regime in which the TA decay kinetics were independent of power and did not show signal from Auger recombination,[56] ensuring that the signal originated from NRs excited by absorption of one photon. During data collection, the samples were stirred constantly.

Light-Driven H_2 Production. Solutions for light-driven H_2 production consisted of 36 nM CdS−CaI complex (1:1 molar ratio) with 200 mM ascorbate (≥99%, Sigma Aldrich) in 50 mM Tris-HCl buffer with 5% glycerol and 5 mM NaCl, pH 7, in 1.5 mL vials sealed with septa. The samples were illuminated with a 405 nm diode laser (Laserglow Technologies) at 5 mW for 10 min. H_2 was detected in the headspace of the vessel using gas chromatography (Agilent Technologies 7820A, molecular sieve 5A column, Ar carrier gas, TCD detector).

RESULTS

Electron Decay Kinetics in CdS NRs. To directly probe the kinetics of relaxation and ET in CdS NRs, we employed TA spectroscopy over a temporal window of 10^{-13}−10^{-6} s with time resolution of ∼200 fs. Upon excitation with a 400 nm pump pulse, TA spectra of CdS NRs exhibit a transient bleach feature at the 472 nm, corresponding to the band gap transition (Supporting Information Figure S3a). This feature originates from filling of the 1S electron state, and its intensity (i.e., magnitude of the negative signal) reflects the photoexcited 1S electron population.[56] The bleach feature is insensitive to the population of the photoexcited holes.[47,57,58] Thus, the kinetics of the band gap bleach are a signature of electron dynamics. In CdS NRs, 1S electrons decay by radiative and nonradiative processes, including electron trapping, recombination with valence band holes, and recombination with trapped holes on the surface. Trap states are symbolized by energy levels shown in light blue in Figure 1.

The band gap bleach signal of CdS α NRs (average diameter = 4.3 nm and average length = 21.5 nm) is relatively long-lived

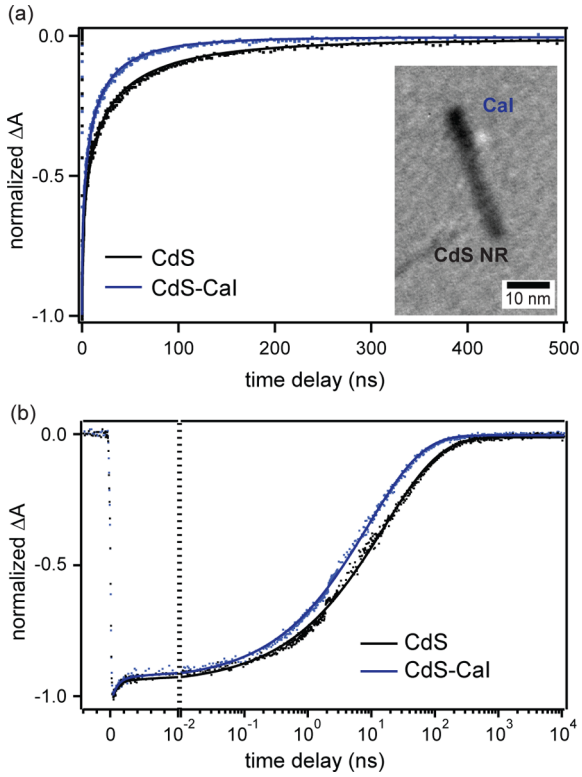

Figure 2. TA kinetics of the band gap feature (472 nm) for CdS NRs (black) and CdS−CaI complexes (molar ratio 1:1, blue). The CdS−CaI complexes have a shorter photoexcited electron lifetime due to ET from CdS to CaI. The kinetics are plotted (a) with a linear time axis or (b) with a split time axis that is linear for the first 10 ps and logarithmic thereafter. The solid lines correspond to fit models as described in the text. Inset in (a): TEM image of a CdS−CaI complex obtained using a negative stain. The light contrast corresponds to CaI, and the dark corresponds to CdS.

and does not fully decay to baseline until around 1.2 μs (Figure 2, black trace). The slow electron decay in CdS NRs is accompanied by weak band gap photoluminescence and strong trap-state emission.[47] This behavior has been attributed to slow recombination of the delocalized electron with the localized, trapped holes.[47,49,59] As evident from the TA signal plotted using a logarithmic time axis (Figure 2b), the electron decay kinetics in CdS NRs cannot be described with a single exponential function. Such behavior is commonly observed with semiconductor nanocrystals.[60−63] The TA kinetics of CdS NRs in Figure 2 can be fit with a sum of a single exponential with a 0.85 ps lifetime (6% of the decay) and a stretched exponential with a time constant of 18.2 ns and a stretching exponent of 0.49 (94%). Similar behavior was recently reported for CdS NRs with long-chain organic ligands on the surface.[64] The stretched exponential fit suggests a distribution of electron decay rates in CdS NRs, the cause of which is not well understood.[64,65] In the absence of a detailed physical model for the CdS NR electron decay kinetics, we focused on quantities that depend only on signal intensity:[66,67] the average lifetime, defined as

$$\bar{\tau} = \frac{\int_0^\infty t \times \Delta A(t)\, dt}{\int_0^\infty \Delta A(t)\, dt} \quad (1)$$

and the time-averaged decay rate constant, defined as

dx.doi.org/10.1021/ja413001p | J. Am. Chem. Soc. 2014, 136, 4316−4324

$$\bar{k} = \frac{1}{\int_0^\infty \Delta A(t)\, dt} \quad (2)$$

where $\Delta A(t)$ is normalized so that $\Delta A(0) = 1$. For the purposes of integration of the ΔA signal, we can use any function that fits the kinetic data well (Supporting Information Figure S6). To verify that the results were not strongly dependent on the fitting equation, we compared the single exponential plus stretched exponential fit, described above, to a 5-exponential fit. The calculations of $\bar{\tau}$ and $\bar{k}$ for CdS NRs using the two different fit functions are detailed in the Supporting Information (section V) and included in Tables S1 and S2, and the results are very similar. The electron decay kinetics of the CdS NRs shown in Figure 2 are characterized by the average lifetime $\bar{\tau}$ of 118 ns and the average decay rate constant $\bar{k}_{CdS}$ of 2.8×10^7 s^{-1}.

ET Kinetics in CdS−CaI Complexes. As we described previously,[19] the negatively charged 3-MPA ligands on CdS allow electrostatic binding to a positively charged surface on CaI. The electrostatic binding likely results in a Poisson distribution of populations.[19] For an average molar ratio of 1:1, 37% of CdS NRs have one CaI moiety attached, 37% have no CaI, and 26% have two or more CaI. TEM images of CdS−CaI complexes obtained using a negative stain (Figures 2a and Supporting Information S2) allow us to directly visualize the complexes because NRs appear dark and CaI molecules appear bright. The images in Supporting Information Figure S2 are consistent with the Poisson distribution model and reflect the heterogeneity of populations, with some CdS NRs having no CaI moieties attached, some having one, and some having multiple.

When CdS NRs were mixed with CaI in a 1:1 molar ratio, the CdS NR band gap bleach feature decayed to baseline more quickly (Figure 2) due to ET to CaI. Because CaI does not have absorptive features with intensities comparable to the strength of the CdS bleach feature,[68] no additional transient features were found in the ΔA spectrum (Supporting Information Figure S3b). In the TA experiment, each NR was excited very infrequently because of the low pump pulse repetition rate (500 s^{-1}), low pulse energy, and constant stirring that rapidly moved the sample through the excitation beam. Consequently, the CdS−CaI sample exhibited no changes in absorption intensity or bleach kinetics over a period of several hours in the TA experiment, indicating that there was no sample precipitation or significant electron accumulation on CaI (Supporting Information Figure S4). Because H_2 production requires two sequential electrons and the experiment was carried out under conditions of low excitation frequency, the sample was not under catalytic turnover conditions, allowing the TA experiment to isolate the one electron transfer step from the CdS NR to CaI.

As shown in Figure 2b, the electron decay kinetics of CdS and CdS−CaI virtually overlap in the picosecond regime, and ET to CaI primarily occurred in the nanosecond time window. The decay kinetics of CdS−CaI can be fit with similar functional forms as CdS electron decay kinetics: a single exponential with a 1.6 ps lifetime (7% of the decay) plus a stretched exponential with a time constant of 11.7 ns and stretching exponent of 0.51 (93%), or a 5-exponential decay (see Supporting Information, section V). The average lifetime of the photoexcited electrons in CdS−CaI, shown in Figure 2, is 62 ns. Because of the distribution of decay rates in CdS, it is not obvious whether k_{ET} to CaI is also heterogeneous. An additional complication is the Poisson distribution of CaI:CdS ratios in the sample. Therefore, to characterize ET kinetics, we again used quantities that depend only on signal intensity.[66,67] Specifically, we focused on QE_{ET} and a time-averaged ET rate constant ($\bar{k}_{ET}$):

$$QE_{ET} = \frac{\bar{k}_{ET}}{\bar{k}_{CdS} + \bar{k}_{ET}} = 1 - \frac{\int_0^\infty \Delta A_{CdS-CaI}(t)\, dt}{\int_0^\infty \Delta A_{CdS}(t)\, dt} \quad (3)$$

$$\bar{k}_{ET} = \bar{k}_{CdS-CaI} - \bar{k}_{CdS} = \frac{1}{\int_0^\infty \Delta A_{CdS-CaI}(t)\, dt} - \frac{1}{\int_0^\infty \Delta A_{CdS}(t)\, dt} \quad (4)$$

where $\bar{k}_{CdS-CaI}$ is the time-averaged decay rate constant for the CdS−CaI complexes. As detailed in Supporting Information Table S1, we found the value of $\bar{k}_{ET}$ to be 2.0×10^7 s^{-1} with a QE_{ET} value of 42%.

ET Kinetics for Varying CaI:CdS Molar Ratios. Figure 3 shows how ET kinetics (with 300 ps time resolution) depend on the average number of CaI moieties per CdS NR (CaI:CdS). The CdS NR concentration was held constant, and the CaI concentration was varied to obtain the values of CaI:CdS ranging from 0.9:1 to 5.7:1. For these experiments, we used longer NRs (CdS β, average length = 32.0 nm) to increase the area available for CaI adsorption. With the estimated NR surface area of 470 nm^2, 6 CaI moieties could adsorb onto the CdS NR surface without approaching saturation of the available surface area.[19] The NR diameters of CdS β were very similar to those of CdS α, resulting in similar steady-state absorption spectra (Supporting Information Figure S1), a TA bleach peak that is blue-shifted by only 2 nm, and a similar driving force for

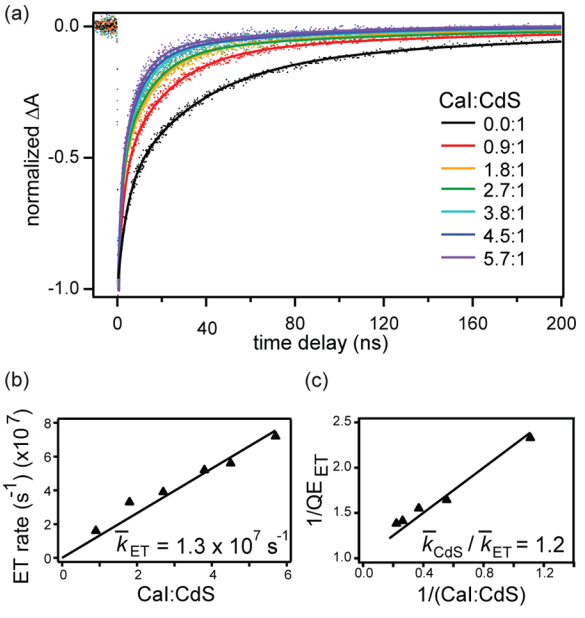

Figure 3. (a) TA decay kinetics (at 470 nm) of CdS−CaI samples with varying values of CaI:CdS (average number of CaI moieties per CdS NR) and constant CdS NR concentration. The kinetics show that with increasing CaI:CdS, the CdS electron decay occurs more quickly, corresponding to increasing ET signal. (b) ET rate versus CaI:CdS, revealing the value of $\bar{k}_{ET}$, as described in the text. (c) The inverse of the QE_{ET} versus the inverse of CaI:CdS. A linear fit to eq 6 reveals the value of $\bar{k}_{CdS}/\bar{k}_{ET}$.

dx.doi.org/10.1021/ja413001p | J. Am. Chem. Soc. 2014, 136, 4316−4324

ET. Figure 3a shows the TA decay kinetics at 470 nm and the triple-exponential decay functions that fit the data well (Supporting Information Table S3b). The average excited-state electron lifetimes ($\bar{\tau}$) decreased with increasing values of CaI:CdS, ranging from 93 ns with 0.9:1 ratio to 40 ns with 5.7:1 ratio. Similar results were obtained using a narrower range of ratios with CdS α (Supporting Information Figures S7 and S8 and Table S3a). When the average molar ratio of CaI and CdS NRs is not 1:1, $\bar{k}_{ET}$ and $\bar{k}_{CdS-CaI}$ (time-averaged *rate constants*) in eq 4 are replaced by the average ET *rate* and the average electron decay *rate* in CdS−CaI, respectively. The latter is determined by integrating the TA signal according to eq 4. Figure 3b shows that the average ET rate scales approximately linearly with the value of CaI:CdS in this range of ratios. Thus, we can write that average ET rate = $\bar{k}_{ET} \times$ (CaI:CdS) to obtain a value of $\bar{k}_{ET}$ from a broader data set than the one shown in Figure 2. From the linear fit in Figure 3b, we obtain a $\bar{k}_{ET}$ value of 1.3×10^7 s^{-1}, which is within a factor of 2 of the value for the CdS−CaI (1:1) sample in Figure 2.

To account for the varying values of CaI:CdS, QE_{ET} can be written as:

$$QE_{ET} = \frac{\bar{k}_{ET} \times (\text{CaI:CdS})}{\bar{k}_{CdS} + \bar{k}_{ET} \times (\text{CaI:CdS})} \quad (5)$$

As shown in Supporting Information Figure S8a, QE_{ET} increases with increasing CaI:CdS, but above a ratio of 1:1, the dependence of QE_{ET} on CaI:CdS is relatively weak because $\bar{k}_{CdS}$ is within the same order of magnitude as $\bar{k}_{ET}$. QE_{ET} reaches a value of 77% at the ratio of 5.7:1. To obtain the ratio ($\bar{k}_{CdS}/\bar{k}_{ET}$), eq 5 can be rearranged to

$$\frac{1}{QE_{ET}} = \left(\frac{\bar{k}_{CdS}}{\bar{k}_{ET}}\right)\left(\frac{1}{\text{CaI:CdS}}\right) + 1 \quad (6)$$

The plot of $1/QE_{ET}$ versus 1/(CaI:CdS) yields the $\bar{k}_{CdS}/\bar{k}_{ET}$ value of 1.2 (Figure 3c), which is consistent with our findings in Figure 2, where the value of $\bar{k}_{CdS}/\bar{k}_{ET}$ was 1.4.

TA Kinetics in CdS NR Complexes with Inactivated CaI. To examine the relationship between the H-cluster properties and the CdS→CaI ET behavior, we measured the ET kinetics between CdS NRs and CaI variants that were not catalytically active due to modifications at the H-cluster. The first variant was an immature form of CaI (CaI^{Im}), which, by analogy to an immature form of HydA1 from *Chlamydomonas reinhardtii* prepared from similar expression conditions,[52,53] is thought to lack the $2Fe_H$ subsite of the H-cluster. The second variant was active CaI treated with carbon monoxide (CaI^{CO}). CO treatment has been shown to reversibly inhibit hydrogenase activity.[69,70] For both variants, the accessory F-clusters remain intact. For CaI^{Im}, $2Fe_H$ subsite biosynthesis is impeded by the absence of maturase factors, but integrity of the accessory F-clusters is not believed to be affected because they are biosynthesized by the housekeeping machinery.[71] The presence of the F-clusters was confirmed by Fe analysis of Ca^{Im}. For CaI^{CO}, CO binding has been demonstrated to occur at the $2Fe_H$ subsite of the H-cluster,[72,73] and further studies on [NiFe]-hydrogenases demonstrated that CO binding does not perturb the redox potential of the F-clusters.[74] Both CaI^{Im} and CaI^{CO} therefore are excellent candidates to examine the role of the H-cluster in the interfacial ET kinetics.

In Figure 4a, we compare the TA band gap signal decay kinetics for CdS NRs (sample α), CdS−CaI, and CdS−CaI^{Im} complexes (both with a 1:1 molar ratio). The average electron lifetime $\bar{\tau}$ of CdS−CaI^{Im} (82 ns) is longer than that of CdS−CaI (63 ns), but still clearly shorter than that of CdS NRs without any form of CaI ($\bar{\tau}$ = 96 ns). The resulting $\bar{k}_{ET}$ in CdS−CaI^{Im} is 8.6×10^6 s^{-1} with a QE_{ET} of 29% (Supporting Information Table S4). These data demonstrate that CaI^{Im} is capable of accepting electrons from CdS NRs.

There may be subtle structural differences between CaI with a fully assembled H-cluster and CaI^{Im} that result in slightly different ET rates and efficiencies. To minimize the number of variables in the comparison between active and inactive CaI, we performed TA experiments on the inhibited CdS−CaI^{CO}. We verified that CO incubation inactivated CaI by carrying out photochemical H_2 production experiments on CO-incubated and Ar-incubated CdS−CaI complexes. Unlike the CdS−CaI complexes under Ar, CdS−CaI^{CO} did not produce a detectable amount of H_2. The results of TA experiments on CdS NRs, CdS−CaI incubated under Ar (active), and CdS−CaI^{CO} (inactive) are shown in Figure 4b. CO incubation has no effect on the TA signal of CdS NRs alone (Supporting Information Figure S5). Remarkably, the decay trace of CdS−CaI^{CO} is also almost identical to that of CdS−CaI. In Figure 4b, for CdS−CaI^{CO}, $\bar{k}_{ET}$ is 1.7×10^7 s^{-1} and QE_{ET} is 44% (for CdS−CaI, $\bar{k}_{ET}$ is 1.8×10^7 s^{-1} and QE_{ET} is 44%).

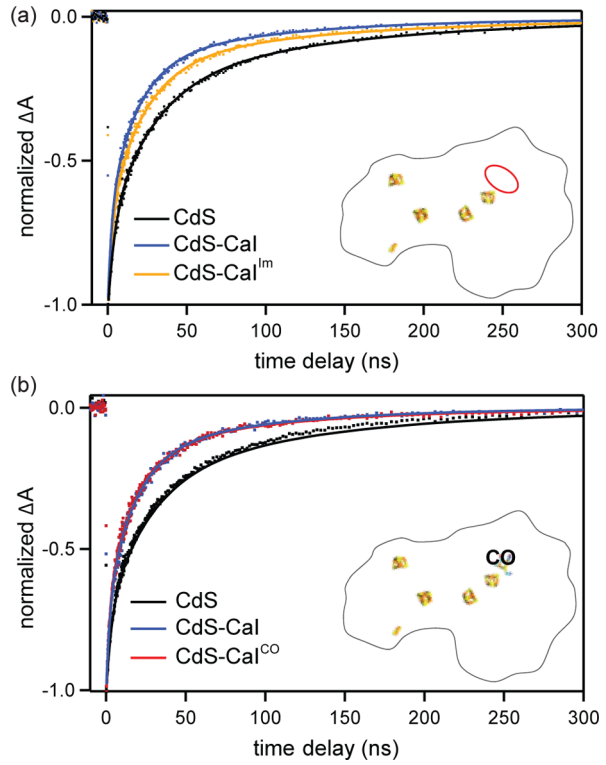

Figure 4. (a) CdS band gap (472 nm) bleach decay kinetics for CdS NRs (black), CdS−CaI (blue), and CdS−CaI^{Im} complexes (orange). Even though it lacks the $2Fe_H$ subsite of the H-cluster, CaI^{Im} can accept electrons from CdS. Inset: Schematic representation of CaI^{Im} emphasizing the missing $2Fe_H$ subsite of the H-cluster (red circle). (b) CdS band gap bleach decay kinetics for CdS NRs (black), CdS−CaI in an Ar atmosphere (blue), and CdS−CaI^{CO} complexes prepared in a CO atmosphere that inactivates the H-cluster (red). Remarkably, CO deactivation does not change the kinetics of ET. Inset: Schematic representation of CaI^{CO} emphasizing the CO binding to the $2Fe_H$ subsite of the H-cluster.

dx.doi.org/10.1021/ja413001p | J. Am. Chem. Soc. 2014, 136, 4316−4324

DISCUSSION

Competition between ET and Electron Relaxation in CdS−CaI Complexes. Our measurements of electron decay kinetics in CdS NRs and CdS−CaI complexes reveal that the electron relaxation in CdS by radiative and nonradiative recombination and ET from CdS to CaI occur with very similar rates, with both $\bar{k}_{CdS}$ and $\bar{k}_{ET} \approx 10^7$ s^{-1}. Thus, the two processes are in direct kinetic competition and occur with similar probabilities. This results in a QE_{ET} of 42%, meaning that only 42% of photoexcited electrons are available for H_2 generation. According to eq 3, to increase QE_{ET}, it would be necessary to either increase $\bar{k}_{ET}$ or decrease $\bar{k}_{CdS}$. Maintaining a 1:1 CaI:CdS molar ratio, a 10-fold increase in $\bar{k}_{ET}/\bar{k}_{CdS}$ would increase the QE_{ET} from 42% to 89%, and a 100-fold increase in $\bar{k}_{ET}/\bar{k}_{CdS}$ would yield a QE_{ET} of 99%. Given the remarkable tunability of the surface and electronic structure of semiconductor nanocrystals, it is entirely feasible that the value of $\bar{k}_{ET}/\bar{k}_{CdS}$ could be changed dramatically through rational structural modifications. For example, in nanocrystal-based electron transfer systems where ET occurred through molecular linkers/surface-capping ligands, gains in ET rate were achieved by decreasing the length of surface-capping ligands.[75,76] Alternatively, using nanocrystals with longer excited-state lifetimes could lead to a higher value of $\bar{k}_{ET}/\bar{k}_{CdS}$. It has been shown that band engineering can be used to achieve long-lived excited states in nanocrystals by formation of charge-separating type-II interfaces.[6,77,78]

We found that the rate of ET and the value of QE_{ET} from CdS NRs to CaI moieties increased when the value of the molar ratio of CaI to CdS NRs increased from 1:1 to several CaI molecules per NR (Figure 3). The linear increase of ET rate with increasing CaI:CdS ratio and a good fit to eq 6 (Figure 3b) demonstrate that the CaI moieties act as independent electron acceptors. The increase in ET rate is a result of the single, delocalized photoexcited electron localizing in a CaI moiety more quickly when there are multiple electron acceptors available. Because the values of $\bar{k}_{CdS}$ and $\bar{k}_{ET}$ are similar, the gains in QE_{ET} with increasing CaI:CdS ratio are, relatively speaking, not very significant. For example, to double QE_{ET} from 42% to 84%, the CaI:CdS molar ratio would need to increase from 1:1 to 6.3:1. In this scenario, twice as many electrons removed from CdS would be divided among 6 times as many CaI moieties, effectively reducing the value of QE_{ET} per CaI from 42% (1:1) to 13% (6.3:1). Because two electrons are required for each H_2, increasing CaI:CdS should have a detrimental effect on the quantum yield of H_2 ($QY(H_2)$) at these values of $\bar{k}_{CdS}$ and $\bar{k}_{ET}$. Even though a higher fraction of electrons is harvested from the photoexcited CdS NRs, the probability of transferring two electrons to the same CaI moiety decreases. This effect is particularly important if photoexcitation rates are relatively low, allowing the first electron bound at the H-cluster to decay before the second electron arrives. The effect of competition for electrons among multiple CaI moieties is evident in our previously reported measurements of H_2 generation using CdS−CaI complexes with varying values of CaI:CdS. The amount of H_2 produced decreased with increasing CaI:CdS above 1:1, and the amount of H_2 produced scaled linearly with the population of 1:1 complexes in the sample.[19]

Our measurements of ET kinetics demonstrate that the detrimental effect of increasing the value of CaI:CdS is ultimately a consequence of the similarity of the $\bar{k}_{CdS}$ and $\bar{k}_{ET}$ values. Examination of eqs 5 and 6 reveals that an increase in the number of CaI moieties per CdS NR would be beneficial for H_2 production if ET were significantly slower than electron decay in the nanocrystal. For example, if the value of $\bar{k}_{ET}/\bar{k}_{CdS}$ were 0.1, QE_{ET} would be 9% at a molar ratio of 1:1, and 18% at a molar ratio of 2:1. This would result in no change in the number of electrons transferred per CaI moiety, and doubling the CaI:CdS ratio would be beneficial to $QY(H_2)$.

Electron Pathways in H_2 Production. Our measurements of ET dynamics in complexes of CdS NRs with catalytically inactive CaI allow us to assemble a more detailed picture of the pathway that electrons transferred from CdS NRs undergo to eventually form the H−H bond. We have previously shown that CdS−CaI complexes form via a biomimetic interaction between the negatively charged surface of CdS NRs capped with 3-MPA and the positively charged surface on the CaI moiety.[19] The F-cluster closest to that surface is the distal [4Fe−4S] cluster.[38,79] Thus, we hypothesized that the photochemical H_2 production in CdS−CaI complexes occurs via electron injection at the distal F-cluster and electron transport to the H-cluster, in analogy to *in vivo* Fd-mediated H_2 production (Figure 5).[19] Within this model, provided that inactivation of the H-cluster does not change the secondary structure of CaI or the locations and electronic properties of the F-clusters, the value of k_{ET} should be governed by the structure and electronic properties in the vicinity of the distal F-cluster, and not depend strongly on the properties of the H-cluster. The TA kinetic data showed that interfacial ET between CdS and CaI was unaffected by CO binding (Figure 4b). Furthermore, ET proceeds in the absence of the $2Fe_H$ subsite of the H-cluster (Figure 4a), demonstrating that an intact H-cluster is not necessary for interfacial ET. These experiments provide strong evidence for our hypothesis that photochemical H_2 production involves electron transport through biomimetic

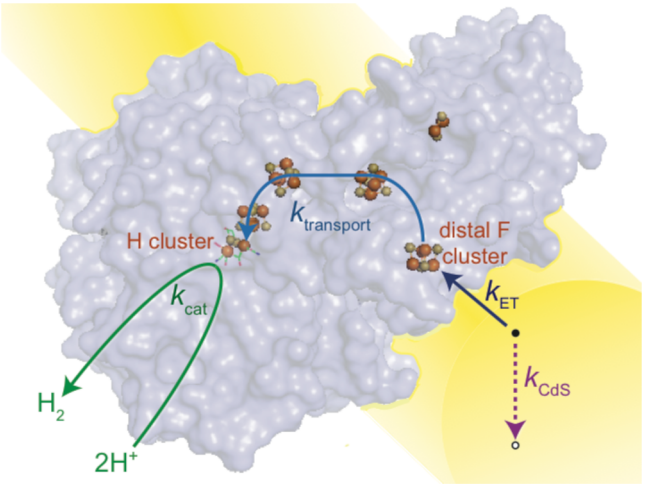

Figure 5. Schematic of the electron pathway resulting in H_2 generation by photoexcited CdS−CaI complexes. The enzyme surface is shown in blue with the Fe and S atoms of the F-clusters and the H-cluster shown as orange and yellow spheres, respectively. Enzyme coordinates are from CpI (PDB ID: 3C8Y), which has high homology and sequence similarity with CaI. The CdS NR surface is shown in yellow and surface-capping ligands are omitted for clarity. The rate of internal electron decay in CdS is denoted by k_{CdS}, the rate of electron injection from CdS to CaI by k_{ET}, the rate of electron transport through CaI to the H-cluster by $k_{transport}$, and the rate of H_2 production by k_{cat}.

dx.doi.org/10.1021/ja413001p | J. Am. Chem. Soc. 2014, 136, 4316−4324

pathways in CdS−CaI complexes. Because the ET does not occur preferentially to catalytically active CaI, but occurs with equal probability to any CaI, our data imply that the overall $QY(H_2)$ includes losses due to ET to inactive CaI that may be present in the sample.[44] We note that TA measurements are uniquely suited to detect the nanosecond electron injection from CdS to CaI in both catalytically active and inactive complexes. Despite the similar midpoint potentials of the F- and H-clusters (−420 and −400 mV at pH 8, respectively),[80] TA experiments allow us to decouple the observation of electron injection from catalysis.

Figure 5 illustrates the complicated pathways that electrons photoexcited in CdS take to H_2. In previous H_2 production experiments with CdS−CaI complexes, the amount of H_2 generated increased linearly with photon flux, indicating that the reaction was photon-limited and the inherent catalytic turnover rate (k_{cat}) was not reached.[19] Under photon-limited conditions, the efficiency with which photoexcited electrons can be transferred from CdS to CaI (QE_{ET}) is a critical parameter in determining the amount of H_2 produced. QE_{ET} in turn depends on k_{ET}/k_{CdS}, as described above. Once an electron has been injected into CaI, it is transported to the active site with the rate constant $k_{transport}$. If all of the electrons transferred from CdS to CaI were utilized in catalysis, the values of QE_{ET} and $QY(H_2)$ would be equal. (The definition of $QY(H_2)$ takes into account that two electrons are required for each H_2 molecule.) In CdS−CaI complexes, $QY(H_2)$ is 2 times lower than QE_{ET}, suggesting that there are additional factors that limit the H_2 production rate. One possible cause is the distribution of the number of CaI moieties per CdS NR,[19] including the presence of complexes with ratios greater than 1:1, in which competition for electrons between CaI moieties on the same NR decreases H_2 production efficiency. Another possibility is ET to catalytically inactive CaI that may be present in the sample,[44] as evidenced by the ability of inactive variants of CaI to accept electrons from CdS NRs. Additional candidates for rate-limiting processes include: back-ET, which is the predominant pathway for some [FeFe]-hydrogenases at higher pH values;[81,82] electron and proton transport steps within CaI;[82−84] covalent bond formation;[30,85] and hole scavenging.[86,87]

Value of $\bar{k}_{ET}$ in CdS−CaI Complexes. The value of $\bar{k}_{ET}$ we measured for electron injection from CdS NRs to CaI (10^7 s^{-1}) is in contrast to much faster ET from nanocrystals to molecules or metal particles adsorbed directly on the nanocrystal surface, usually observed to be in the 10^9−10^{12} s^{-1} range.[7] To understand why the ET rate between CdS NRs and CaI is relatively slow, we consider the charge transfer interface (Figure 5). Because a crystal structure of CaI has not yet been obtained, we use the structure of [FeFe]-hydrogenase I from *Clostridium pasteurianum* (CpI) (PDB ID: 3C8Y) as an analogue.[79] CpI has 82% sequence similarity with CaI, and all 22 cysteine residues in CpI are conserved in CaI, suggesting similar binding and location of the F-clusters.[88] The distal F-cluster is 4 Å away from the positive outer surface of the protein. However, due to the surface curvature of the Fd-binding pocket of the enzyme, the closest point of contact between CaI and CdS may be up to 8 Å away from the distal F-cluster. Additionally, electrons may tunnel through the ∼5 Å long NR-surface-capping ligand (3-MPA) to reach CaI. In redox enzymes, relatively slow ET rates are common because of electron tunneling over long distances.[89,90] An ET rate constant of 10^7 s^{-1} is consistent with the considerable tunneling distance between CdS and the distal F-cluster. The value of k_{ET} may be increased by modifying the structure and electronic properties of the nanocrystals, including the surface-capping ligands.

Considering that electron injection from CdS into the distal F-cluster of CaI is followed by electron transport via the redox chain of iron−sulfur clusters, an increase in k_{ET} is in principle only beneficial until k_{ET} matches $k_{transport}$. Any further increase would result in a kinetic bottleneck inside CaI, rather than at the CdS−CaI interface, and possibly even back-ET from iron−sulfur clusters close to the CdS−CaI interface. We can estimate the maximum value of $k_{transport}$ through the iron−sulfur clusters in CaI by applying the Moser−Dutton model of electron transfer in proteins.[89,91] In this Marcus theory-based model, rates of ET between cofactors in a redox transport chain depend exponentially on tunneling distances, driving force for ET (ΔG_{ET}), and reorganization energy (λ). Without detailed knowledge of ΔG_{ET} and λ, we can determine the maximum rate of electron transport ($k_{transport,max}$), which occurs when $-\Delta G_{ET} = \lambda$. $k_{transport,max}$ depends only on internuclear cluster-to-cluster distances (R)[92] as detailed in section VII of the Supporting Information. The resulting value of $k_{transport,max}$ calculated using Supporting Information eqs S4 and S5 is 2.2×10^9 s^{-1}. This means that in an effort to increase the value of k_{ET} to increase the efficiency of H_2 production, it is not necessary to aim for values as high as those obtained in nanocrystal−molecule complexes. Increasing the k_{ET} value to 10^9 s^{-1} would lead to QE_{ET} of 99% if the value of k_{CdS} remained unchanged, and values of k_{ET} above 10^9 s^{-1} are not likely to be beneficial.

Comparison of CdS−CaI with CdS−Pt Nanoheterostructures. We now contrast the charge transfer behavior of CdS−CaI complexes with that of previously reported CdS−Pt nanoheterostructures, which also photochemically produce H_2.[10,11,15] In such structures, Pt nanoparticles are grown directly on the surfaces of CdS NRs that are synthesized by methods comparable to those used for the CdS NRs in our experiments. To produce H_2, photoexcitation of CdS is followed by ET to Pt, which catalyzes H^+ reduction, while hole scavenging is carried out by molecular electron donors.[10,11,87] ET from CdS to Pt is very fast, with $k_{ET} > 10^{11}$ s^{-1}, and essentially 100% efficient.[59,93,94] Thus, the fraction of photoexcited electrons available for reduction is higher in CdS−Pt than in CdS−CaI structures. Yet, the reported $QY(H_2)$ values for CdS−Pt[10,11] (1−4%) are lower than the 20% reported for CdS−CaI.[19] In Pt-based structures, $QY(H_2)$ increased to 20% when CdSe/CdS core/shell NRs were employed.[10]

On the basis of the intricate kinetics involved in H_2 generation in the CdS−CaI system, we can speculate on the reasons the CdS−CaI system exhibits a relatively high value of $QY(H_2)$ despite a slow and less efficient ET. Because the rate of excitation of CdS NRs during H_2 generation is low (∼10^3 s^{-1})[19] and two electrons are required for each H_2 molecule, it is important for the singly reduced state to be stable for a relatively long period of time. In CaI, following injection at the distal F-cluster, the first electron is transported over 29 Å through a sequence of electron transfer steps to the active site (H-cluster),[79] where it is captured in a chemically bonded hydride intermediate.[41−43] Considering the large distance over which charge separation occurs, the multistep nature of electron transport, and the relative stability of the hydride, it is very likely that back-ET is quite slow. Long-range charge separation is also likely crucial for photochemical H_2 generation by an all-biological system that couples photosystem I with CaI.[95,96] On the other hand, the first electron used for catalysis

in the CdS−Pt structures is spatially closer to the nanocrystal−catalyst interface and is potentially more likely to recombine with a hole in the nanocrystal by back-ET. The higher $QY(H_2)$ achieved in CdSe/CdS−Pt structures is probably due to improved charge separation that reduces the rate of back-ET.[10,97] These examples illustrate that high QE_{ET} from the nanocrystal to the catalyst does not guarantee high values of $QY(H_2)$, and that the intricacies of the catalytic mechanism following ET need to be considered in the analysis of the photochemical activity of nanocrystal-based hybrids.

CONCLUSIONS

We have examined the kinetics of electron transfer (ET) between light-absorbing CdS nanorods (NRs) and the redox enzyme [FeFe]-hydrogenase I from *Clostridium acetobutylicum* (CaI). The ET process is essential for photochemical generation of H_2 mediated by these complexes, and its efficiency defines the upper limit for the quantum yield of H_2 production. We used transient absorption (TA) spectroscopy to measure the rates and efficiencies of ET from CdS to CaI. The ET rate constant was similar to the rate constant for the decay of photoexcited electrons in CdS NRs (both 10^7 s^{-1}), resulting in 42% efficient ET in complexes with the average CdS:CaI ratio of 1:1. The efficiency of ET could be improved in the future by a combination of increased ET rate and decreased rate of electron decay in the nanocrystal. Both goals may be achievable through structural modification of nanocrystals. Increasing the average number of CaI moieties per CdS NR resulted in competition for electrons. This ultimately leads to decreased H_2 production efficiency. The ET behavior in catalytically inactive CdS−CaI^{Im} and CdS−CaI^{CO} was similar to that in active CdS−CaI complexes, demonstrating that electron injection occurred into a distal F-cluster of CaI in a manner analogous to the natural function of CaI. These insights into the kinetics of electron injection from CdS NRs to CaI allow us to begin to assemble a picture of the complex electron pathways involved in photochemical H_2 generation and to understand how the rates of sequential steps along the path determine the overall efficiency of H_2 production.

ASSOCIATED CONTENT

Supporting Information

Sample characterization, transient absorption spectra of CdS with and without CaI, characterization of the stability of CdS−CaI samples in the TA experiments, TA kinetics of CdS NRs under CO, fitting of the transient absorption kinetics, TA kinetics of CdS−CaI samples with varying CaI:CdS ratios, and $k_{transport,max}$ calculations. This material is available free of charge via the Internet at http://pubs.acs.org.

AUTHOR INFORMATION

Corresponding Author

gordana.dukovic@colorado.edu

Notes

The authors declare no competing financial interest.

ACKNOWLEDGMENTS

Nanorod synthesis was supported by the NSF CAREER Award no. CHE-1151151 (M.B.W. and G.D.). TA measurements were supported by startup funds from the University of Colorado Boulder and by the U.S. Department of Energy, Office of Basic Energy Sciences, Division of Materials Sciences and Engineering under Award DE-SC0010334 (M.B.W., K.E.S., G.D.). K.A.B., D.W.M., and P.W.K. gratefully acknowledge funding support for CaI preparation and photochemical measurements from the U.S. Department of Energy, Division of Chemical Sciences, Geosciences, and Biosciences, Office of Basic Energy Sciences; and support of the U.S. Department of Energy under Contract no. DE-AC36-08-GO28308 with the National Renewable Energy Laboratory.

REFERENCES

(1) Yin, Y.; Alivisatos, A. P. *Nature* **2005**, *437*, 664.
(2) Burda, C.; Chen, X. B.; Narayanan, R.; El-Sayed, M. A. *Chem. Rev.* **2005**, *105*, 1025.
(3) Bawendi, M. G.; Steigerwald, M. L.; Brus, L. E. *Annu. Rev. Phys. Chem.* **1990**, *41*, 477.
(4) Cozzoli, P. D.; Pellegrino, T.; Manna, L. *Chem. Soc. Rev.* **2006**, *35*, 1195.
(5) Brus, L. *J. Phys. Chem.* **1986**, *90*, 2555.
(6) Talapin, D. V.; Lee, J. S.; Kovalenko, M. V.; Shevchenko, E. V. *Chem. Rev.* **2010**, *110*, 389.
(7) Wilker, M. B.; Schnitzenbaumer, K. J.; Dukovic, G. *Isr. J. Chem.* **2012**, *52*, 1002.
(8) Chen, X. B.; Shen, S. H.; Guo, L. J.; Mao, S. S. *Chem. Rev.* **2010**, *110*, 6503.
(9) Acharya, K. P.; Khnayzer, R. S.; O'Connor, T.; Diederich, G.; Kirsanova, M.; Klinkova, A.; Roth, D.; Kinder, E.; Imboden, M.; Zamkov, M. *Nano Lett.* **2011**, *11*, 2919.
(10) Amirav, L.; Alivisatos, A. P. *J. Phys. Chem. Lett.* **2010**, *1*, 1051.
(11) Berr, M.; Vaneski, A.; Susha, A. S.; Rodriguez-Fernandez, J.; Doblinger, M.; Jackel, F.; Rogach, A. L.; Feldmann, J. *Appl. Phys. Lett.* **2010**, *97*, 093108.
(12) Shemesh, Y.; Macdonald, J. E.; Menagen, G.; Banin, U. *Angew. Chem., Int. Ed.* **2011**, *50*, 1185.
(13) Zhu, H.; Song, N.; Lv, H.; Hill, C. L.; Lian, T. *J. Am. Chem. Soc.* **2012**, *134*, 11701.
(14) Bang, J. U.; Lee, S. J.; Jang, J. S.; Choi, W.; Song, H. *J. Phys. Chem. Lett.* **2012**, *3*, 3781.
(15) Vaneski, A.; Susha, A. S.; Rodriguez-Fernandez, J.; Berr, M.; Jackel, F.; Feldmann, J.; Rogach, A. L. *Adv. Funct. Mater.* **2011**, *21*, 1547.
(16) Das, A.; Han, Z. J.; Haghighi, M. G.; Eisenberg, R. *Proc. Natl. Acad. Sci. U.S.A.* **2013**, *110*, 16716.
(17) Han, Z.; Qiu, F.; Eisenberg, R.; Holland, P. L.; Krauss, T. D. *Science* **2012**, *338*, 1321.
(18) Brown, K. A.; Dayal, S.; Ai, X.; Rumbles, G.; King, P. W. *J. Am. Chem. Soc.* **2010**, *132*, 9672.
(19) Brown, K. A.; Wilker, M. B.; Boehm, M.; Dukovic, G.; King, P. W. *J. Am. Chem. Soc.* **2012**, *134*, 5627.
(20) Greene, B. L.; Joseph, C. A.; Maroney, M. J.; Dyer, R. B. *J. Am. Chem. Soc.* **2012**, *134*, 11108.
(21) Reisner, E.; Powell, D. J.; Cavazza, C.; Fontecilla-Camps, J. C.; Armstrong, F. A. *J. Am. Chem. Soc.* **2009**, *131*, 18457.
(22) Reisner, E.; Fontecilla-Camps, J. C.; Armstrong, F. A. *Chem. Commun.* **2009**, 550.
(23) Wang, F.; Wang, W. G.; Wang, X. J.; Wang, H. Y.; Tung, C. H.; Wu, L. Z. *Angew. Chem., Int. Ed.* **2011**, *50*, 3193.
(24) Wang, F.; Wang, W. G.; Wang, H. Y.; Si, G.; Tung, C. H.; Wu, L. Z. *ACS Catal.* **2012**, *2*, 407.
(25) Li, C. B.; Li, Z. J.; Yu, S.; Wang, G. X.; Wang, F.; Meng, Q. Y.; Chen, B.; Feng, K.; Tung, C. H.; Wu, L. Z. *Energy Environ. Sci.* **2013**, *6*, 2597.
(26) Wen, F.; Li, C. *Acc. Chem. Res.* **2013**, *46*, 2355.
(27) Armstrong, F. A.; Hirst, J. *Proc. Natl. Acad. Sci. U.S.A.* **2011**, *108*, 14049.
(28) Fontecilla-Camps, J. C.; Volbeda, A.; Cavazza, C.; Nicolet, Y. *Chem. Rev.* **2007**, *107*, 5411.
(29) De Lacey, A. L.; Fernandez, V. M.; Rousset, M.; Cammack, R. *Chem. Rev.* **2007**, *107*, 4304.

(30) Tard, C.; Pickett, C. J. *Chem. Rev.* **2009**, *109*, 2245.
(31) Siegbahn, P. E. M.; Tye, J. W.; Hall, M. B. *Chem. Rev.* **2007**, *107*, 4414.
(32) English, C. M.; Eckert, C.; Brown, K.; Seibert, M.; King, P. W. *Dalton Trans.* **2009**, 9970.
(33) Adams, M. W. W. *Biochim. Biophys. Acta, Bioenerg.* **1990**, *1020*, 115.
(34) Peters, J. W. *Curr. Opin. Struct. Biol.* **1999**, *9*, 670.
(35) Baffert, C.; Sybirna, K.; Ezanno, P.; Lautier, T.; Hajj, V.; Meynial-Salles, I.; Soucaille, P.; Bottin, H.; Leger, C. *Anal. Chem.* **2012**, *84*, 7999.
(36) Demuez, M.; Cournac, L.; Guerrini, O.; Soucaille, P.; Girbal, L. *FEMS Microbiol. Lett.* **2007**, *275*, 113.
(37) Benemann, J. R.; Berenson, J. A.; Kaplan, N. O.; Kamen, M. D. *Proc. Natl. Acad. Sci. U.S.A.* **1973**, *70*, 2317.
(38) Peters, J. W.; Lanzilotta, W. N.; Lemon, B. J.; Seefeldt, L. C. *Science* **1998**, *282*, 1853.
(39) Hexter, S. V.; Grey, F.; Happe, T.; Climent, V.; Armstrong, F. A. *Proc. Natl. Acad. Sci. U.S.A.* **2012**, *109*, 11516.
(40) Vincent, K. A.; Parkin, A.; Armstrong, F. A. *Chem. Rev.* **2007**, *107*, 4366.
(41) Capon, J. F.; Gloaguen, F.; Petillon, F. Y.; Schollhammer, P.; Talarmin, J. *Coord. Chem. Rev.* **2009**, *253*, 1476.
(42) Mulder, D. W.; Ratzloff, M. W.; Shepard, E. M.; Byer, A. S.; Noone, S. M.; Peters, J. W.; Broderick, J. B.; King, P. W. *J. Am. Chem. Soc.* **2013**, *135*, 6921.
(43) Barton, B. E.; Rauchfuss, T. B. *Inorg. Chem.* **2008**, *47*, 2261.
(44) Madden, C.; Vaughn, M. D.; Díez-Pérez, I.; Brown, K. A.; King, P. W.; Gust, D.; Moore, A. L.; Moore, T. A. *J. Am. Chem. Soc.* **2012**, *134*, 1577.
(45) Warren, J. J.; Mayer, J. M. *J. Am. Chem. Soc.* **2010**, *132*, 7784.
(46) Greene, B. L.; Joseph, C. A.; Maroney, M. J.; Dyer, R. B. *J. Am. Chem. Soc.* **2012**, *134*, 11108.
(47) Tseng, H. W.; Wilker, M. B.; Damrauer, N. H.; Dukovic, G. *J. Am. Chem. Soc.* **2013**, *135*, 3383.
(48) Robinson, R. D.; Sadtler, B.; Demchenko, D. O.; Erdonmez, C. K.; Wang, L. W.; Alivisatos, A. P. *Science* **2007**, *317*, 355.
(49) Peng, P.; Sadtler, B.; Alivisatos, A. P.; Saykally, R. J. *J. Phys. Chem. C* **2010**, *114*, 5879.
(50) Aldana, J.; Lavelle, N.; Wang, Y.; Peng, X. *J. Am. Chem. Soc.* **2005**, *127*, 2496.
(51) King, P. W.; Posewitz, M. C.; Ghirardi, M. L.; Seibert, M. *J. Bacteriol.* **2006**, *188*, 2163.
(52) Mulder, D. W.; Boyd, E. S.; Sarma, R.; Lange, R. K.; Endrizzi, J. A.; Broderick, J. B.; Peters, J. W. *Nature* **2010**, *465*, 248.
(53) Mulder, D. W.; Ortillo, D. O.; Gardenghi, D. J.; Naumov, A. V.; Ruebush, S. S.; Szilagyi, R. K.; Huynh, B. H.; Broderick, J. B.; Peters, J. W. *Biochemistry* **2009**, *48*, 6240.
(54) Fish, W. W. *Methods Enzymol.* **1988**, *158*, 357.
(55) Rasband, W. S. *ImageJ*; U.S. National Institutes of Health: Bethesda, MD, 1997−2012; http://imagej.nih.gov/ij/.
(56) Klimov, V. I. *Annu. Rev. Phys. Chem.* **2007**, *58*, 635.
(57) Huang, J. E.; Huang, Z. Q.; Jin, S. Y.; Lian, T. Q. *J. Phys. Chem. C* **2008**, *112*, 19734.
(58) Sykora, M.; Petruska, M. A.; Alstrum-Acevedo, J.; Bezel, I.; Meyer, T. J.; Klimov, V. I. *J. Am. Chem. Soc.* **2006**, *128*, 9984.
(59) Wu, K. F.; Zhu, H. M.; Liu, Z.; Rodriguez-Cordoba, W.; Lian, T. Q. *J. Am. Chem. Soc.* **2012**, *134*, 10337.
(60) Knowles, K. E.; McArthur, E. A.; Weiss, E. A. *ACS Nano* **2011**, *5*, 2026.
(61) Jones, M.; Scholes, G. D. *J. Mater. Chem.* **2010**, *20*, 3533.
(62) Zhu, H.; Song, N.; Lian, T. *J. Am. Chem. Soc.* **2011**, *133*, 8762.
(63) van Driel, A. F.; Nikolaev, I. S.; Vergeer, P.; Lodahl, P.; Vanmaekelbergh, D.; Vos, W. L. *Phys. Rev. B* **2007**, *75*, 035329.
(64) Wu, K.; Rodríguez-Córdoba, W. E.; Yang, Y.; Lian, T. *Nano Lett.* **2013**, *13*, 5255.
(65) Sadhu, S.; Patra, A. *J. Phys. Chem. C* **2011**, *115*, 16867.
(66) Lakowicz, J. R. *Principles of Fluorescence Spectroscopy*; Springer: New York, 2006.
(67) Berberan-Santos, M. N.; Bodunov, E. N.; Valeur, B. *Chem. Phys.* **2005**, *315*, 171.
(68) Adams, M. W.; Mortenson, L. E. *J. Biol. Chem.* **1984**, *259*, 7045.
(69) Thauer, R. K.; Kaufer, B.; Zahringe, M.; Jungerma, K. *Eur. J. Biochem.* **1974**, *42*, 447.
(70) Goldet, G.; Brandmayr, C.; Stripp, S. T.; Happe, T.; Cavazza, C.; Fontecilla-Camps, J. C.; Armstrong, F. A. *J. Am. Chem. Soc.* **2009**, *131*, 14979.
(71) Mulder, D. W.; Shepard, E. M.; Meuser, J. E.; Joshi, N.; King, P. W.; Posewitz, M. C.; Broderick, J. B.; Peters, J. W. *Structure* **2011**, *19*, 1038.
(72) Bennett, B.; Lemon, B. J.; Peters, J. W. *Biochemistry* **2000**, *39*, 7455.
(73) Lemon, B. J.; Peters, J. W. *Biochemistry* **1999**, *38*, 12969.
(74) Pershad, H. R.; Duff, J. L. C.; Heering, H. A.; Duin, E. C.; Albracht, S. P. J.; Armstrong, F. A. *Biochemistry* **1999**, *38*, 8992.
(75) Dibbell, R. S.; Watson, D. F. *J. Phys. Chem. C* **2009**, *113*, 3139.
(76) Tagliazucchi, M.; Tice, D. B.; Sweeney, C. M.; Morris-Cohen, A. J.; Weiss, E. A. *ACS Nano* **2011**, *5*, 9907.
(77) Lo, S. S.; Mirkovic, T.; Chuang, C. H.; Burda, C.; Scholes, G. D. *Adv. Mater.* **2011**, *23*, 180.
(78) Zhu, H. M.; Lian, T. Q. *Energy Environ. Sci.* **2012**, *5*, 9406.
(79) Pandey, A. S.; Harris, T. V.; Giles, L. J.; Peters, J. W.; Szilagyi, R. K. *J. Am. Chem. Soc.* **2008**, *130*, 4533.
(80) Adams, M. W. W. *J. Biol. Chem.* **1987**, *262*, 15054.
(81) Parkin, A.; Cavazza, C.; Fontecilla-Camps, J. C.; Armstrong, F. A. *J. Am. Chem. Soc.* **2006**, *128*, 16808.
(82) Cornish, A. J.; Gärtner, K.; Yang, H.; Peters, J. W.; Hegg, E. L. *J. Biol. Chem.* **2011**, *286*, 38341.
(83) Bertrand, P.; Dole, F.; Asso, M.; Guigliarelli, B. *J. Biol. Inorg. Chem.* **2000**, *5*, 682.
(84) Abou Hamdan, A.; Dementin, S.; Liebgott, P. P.; Gutierrez-Sanz, O.; Richaud, P.; De Lacey, A. L.; Rousset, M.; Bertrand, P.; Cournac, L.; Leger, C. *J. Am. Chem. Soc.* **2012**, *134*, 9828.
(85) Cheah, M. H.; Tard, C.; Borg, S. J.; Liu, X.; Ibrahim, S. K.; Pickett, C. J.; Best, S. P. *J. Am. Chem. Soc.* **2007**, *129*, 11085.
(86) Chaudhary, Y. S.; Woolerton, T. W.; Allen, C. S.; Warner, J. H.; Pierce, E.; Ragsdale, S. W.; Armstrong, F. A. *Chem. Commun.* **2012**, *48*, 58.
(87) Berr, M. J.; Wagner, P.; Fischbach, S.; Vaneski, A.; Schneider, J.; Susha, A. S.; Rogach, A. L.; Jackel, F.; Feldmann, J. *Appl. Phys. Lett.* **2012**, *100*, 223903.
(88) Santangelo, J. D.; Dürre, P.; Woods, D. R. *Microbiology* **1995**, *141*, 171.
(89) Moser, C. C.; Keske, J. M.; Warncke, K.; Farid, R. S.; Dutton, P. L. *Nature* **1992**, *355*, 796.
(90) Gray, H. B.; Winkler, J. R. *Proc. Natl. Acad. Sci. U.S.A.* **2005**, *102*, 3534.
(91) Page, C. C.; Moser, C. C.; Chen, X. X.; Dutton, P. L. *Nature* **1999**, *402*, 47.
(92) Moser, C. C.; Page, C. C.; Dutton, P. L. *Photochem. Photobiol. Sci.* **2005**, *4*, 933.
(93) O'Connor, T.; Panov, M. S.; Mereshchenko, A.; Tarnovsky, A. N.; Lorek, R.; Perera, D.; Diederich, G.; Lambright, S.; Moroz, P.; Zamkov, M. *ACS Nano* **2012**, *6*, 8156.
(94) Berr, M. J.; Vaneski, A.; Mauser, C.; Fischbach, S.; Susha, A. S.; Rogach, A. L.; Jackel, F.; Feldmann, J. *Small* **2012**, *8*, 291.
(95) Lubner, C. E.; Grimme, R.; Bryant, D. A.; Golbeck, J. H. *Biochemistry* **2009**, *49*, 404.
(96) Lubner, C. E.; Applegate, A. M.; Knorzer, P.; Ganago, A.; Bryant, D. A.; Happe, T.; Golbeck, J. H. *Proc. Natl. Acad. Sci. U.S.A.* **2011**, *108*, 20988.
(97) Amirav, L.; Alivisatos, A. P. *J. Am. Chem. Soc.* **2013**, *135*, 13049.